INT. J. REMOTE SENSING, 1994, VOL. 15, NO. 11, 2175–2192

Potential observations with EURECA/VEXUVIO imaging spectrometer

S. MATTEI

Consortium for Research on Advanced Remote Sensing Systems (CORISTA), P. le Tecchio 80, 80125, Naples, Italy

S. VETRELLA, A. MOCCIA

University of Naples, Faculty of Engineering, P. le Tecchio 80, 80125, Naples, Italy

A. L. LANE, D. C. PIERI, M. J. ABRAMS

Jet Propulsion Laboratory (JPL), California Institute of Technology, Earth and Space Sciences Division, 4800 Oak Grove Drive, Pasadena, CA, 91109-8099, U.S.A.

and R. BIANCHI

National Research Council of Italy (CNR), Via G. Galilei CP 27, 00044, Frascati (Roma), Italy

(Received 12 February 1993; in final form 30 November 1993)

Abstract. Despite its geological importance, the Earth's volcanic activity has only recently been studied as a global system, with the advent of sophisticated airborne and spaceborne remote sensing systems that safely and economically provide global access at will. Particularly relevant to this approach are global studies of the effects on weather and climate caused by volcanic solid/gaseous products and thermal flux into the environment. To study such time-varying phenomena, observations of volcanic emissions spectral response, acquired simultaneously at a variety of wavelengths from ultra-violet to infra-red, could yield relevant information on the compositions and concentrations of environmentally important components, such as volcanically generated sulphur compounds (e.g., SO_2, H_2SO_4), and on volcanoes thermal behaviour. For this purpose, a multi-band imaging spectrometer, dedicated to volcanological observations (VEXUVIO, Visible EXplorer Ultra Violet Infra-red Observer) has been designed to be flown on-board EURECA (EUropean REtrievable CArrier) spacecraft, to be launched by the European Space Agency on the NASA Space Shuttle in 1996. In order to analyse potential observation scenarios with this sensor, volcanoes active during 1991 were studied using a computer code to simulate VEXUVIO capabilities on-board EURECA. Some parameters, representative of the sensor viewing geometry and of the volcanoes observation conditions, are exploited, and several plots are reported, shown their values during the six-months nominal EURECA mission. Despite the limited science objectives of EURECA program and a tightly constrained operational environment, our simulation demonstrates that a reasonable program of volcanologically interesting time-series observations can be carried out during the planned six-months lifetime of the EURECA mission.

1. Introduction

In the last few years, the international volcanology community has identified several new scientific initiatives related to the applications of remote sensing of active volcanoes (Mouginis-Mark *et al.* 1989, Bianchi *et al.* 1990). One of the most ambitious recommendations is the development of an Earth-probe class mission dedicated to global observations of areas where volcanological phenomena take place. The consensus within the scientific community is that such a dedicated mission would provide a unique opportunity to acquire systematic time-series data on the eruptive behaviour of many active volcanoes world-wide, and in particular, systematic measurements on quantity and nature of gas and thermal behaviour of volcanoes in a variety of geological and tectonic settings.

As a first step in response to that recommendation, the consortium CORISTA (Consortium for the Research on Advanced Remote Sensing Systems), in collaboration with scientists of JPL (Jet Propulsion Laboratory, Pasadena) Geology and Planetology Section, and of CNR-Frascati (National Research Council) Geology Section, submitted a proposal to ASI (Italian Space Agency), which has been accepted, for studying and developing a new multi-spectral sensor dedicated to volcanic observations. This sensor has been proposed to be flown on-board EURECA, an ESA free-flying satellite.

This paper describes the scientific rationale, the instrument concept and the orbital coverage offered by EURECA.

2. Scientific rationale

Despite the large number of volcanoes, their ubiquity, their geological importance and their proximity and effects on population centres, the actual eruption mechanism and how they (sometimes massively) transfer solid/gaseous products and energy into the environment are only poorly understood. It is probably fair to say that volcanoes, though they are the most active global geological system, have never been adequately studied as such, not even in their subaerial manifestations, due to the difficulty of carrying out ground volcanological observations economically and safely on a global scale during eruptions.

A new approach is offered by aerospace remote sensing which allows, using multispectral imaging systems, observations of various volcanic areas as discrete geological entities, easily overcoming problems of extreme hazard and difficult terrain. Systematic and frequent observations of volcanoes at adequate spatial and spectral resolutions provide a unique opportunity to understand volcanism and to clarify the role of volcanoes in influencing weather and climate. Nevertheless, even if airborne observations seem to be preferable, systematic airborne observations on a global scale are logistically and economically difficult, and sometimes dangerous. Orbital platforms offer an efficient compromise among synoptic coverage, frequency of observations, accessibility, resolution, spectral range and economy of effort for gathering quantitative data on large-scale volcanic phenomena (Mouginis-Mark *et al.* 1991, Rothery and Pieri 1993).

A dedicated orbital mission could carry out specific scientific tasks as follows:

(*a*) Monitoring of active volcanoes during periods of non-activity, and particularly leading up to and following eruptions, will be useful in establishing a capability to predict major eruptions. Keys to predicting eruptive patterns which can be quantitatively measured remotely include changes in gas

emissions (both changes in composition and in concentration) and energy flux.

(*b*) Observing emissions of SO_2 one of the primary gases released at volcanic vents. Changes in SO_2 at vent areas, either from vents, fumaroles, or lava ponds, can indicate movement of magma beneath the surface. The ability to monitor SO_2 and aerosol emissions consistently for a number of designated active volcanoes, in active and passive emission stages, will play an important role in developing our understanding of the relation between changes in SO_2 flux and eruptive activity. Some of the gases released at volcanic sites (SO_2, HCl, CO_2, H_2O, HF, H_2S), have accessible spectral signatures, and their detection can yield information on the presence of subsurface magma.

(*c*) A better understanding of the relation between changes in energy flux and eruptive activity can be achieved by remote means. Changes in energy flux have been shown to correspond to changes in the type of volcanic activity (e.g., passive degassing to explosive eruption to lava dome growth) at particular volcanoes.

(*d*) Developing physical models of volcanic activity.

3. Instrument concept

The recent applications of several airborne sensors (TIMS (Abbott 1990), AIS, AVIRIS/TMS (Farrand and Singer 1991), COSPEC (Malinconico 1979, Haulet *et al.* 1977, Casadevall *et al.* 1990) and spaceborne sensors (Landsat-TM (Rothery *et al.* 1988, Pieri *et al.* 1990, Abrams *et al.*, Oppenheimer 1991, Oppenheimer and Rothery 1991, Rothery and Oppenheimer 1991, Oppenheimer *et al.* 1993), TOMS-UV (Krueger 1983), UVIS) to volcanological observations have given a basis for identifying the special requirements of a new sensor dedicated to monitor volcanoes.

The most important requirement is to integrate multiband (Near-IR, Visible, Near-UV) high-resolution imaging and pointing capabilities, in order to simultaneously measure a wide range of physical processes related to volcanic phenomena, such as changes in thermal flux, changes in gas concentrations and compositions nearby volcanoes (IR and visible spectral range), and volcanic SO_2 and aerosols ejected in stratosphere by explosive eruptions, like the Pinatubo's one (near-UV spectral range).

Following the user requirements, a joint effort between CORISTA and JPL was started to design and develop a prototype imaging spectrometer, named VEXUVIO (Visible EXplorer and Ultra Violet Infrared Observer). VEXUVIO is mainly composed of the following units:

(*a*) UV imaging spectrometer operating over 280–420 nm. The spectrometer is coupled with a UV intensified CCD camera providing 700 channels with a spectral resolution of 2–4 Å;

(*b*) Visible CCD video-camera working typically from 400–950 nm. A filter wheel provides the imaging capability in selected spectral bands;

(*c*) Near-infrared CCD camera working from 1·1 to 3·5 μm. A filter wheel provides the imaging capability in different spectral bands;

(*d*) A purely reflective telescope assembly with a panchromatic response from 280 to more than 3500 nm. The telescope is designed for a FOV of about 3·4° by 3·4°, corresponding to an image size of about 30 km by 30 km from an

orbital altitude of $\cong 500$ km. With a high resolution CCD detector (e.g., 1024 by 1024 pixels array), it is possible to obtain a geometric resolution of about 30 m;

(*e*) The instrument door supports a mirror in its inner side and can be held either fully open for nadir observation, or at a 45° tilt with respect to the telescope line of sight. In this case, it is possible to observe the Earth pre-dawn phase, particularly useful for near-IR imaging without sunlight noise. The two axes gimballed steering mirror will provide the point capabilities of the instrument, within $\pm 30°$;

(*f*) Electro-mechanical sub-system which consists of: data interface (I/F), that provides interface and data transfer to the satellite bus; logic and control unit, that contains the micro-processor to perform management of all instrument functions; motor controller, that provides the driver control for the moving part of the instrument; power supply; mass memory, that is an already space-qualified Solid State Recorder (SSR).

The sensor block diagram, the nadir and pre-dawn operating modes are shown in figures 1, 2 and 3 respectively.

4. EURECA mission

EURECA, the EUropean REtrievable CArrier (Nellessen 1991, 1986), is a free-flying retrievable platform, which is part of the Columbus precursor flights programme. Although it is primarily devoted to research in the fields of material and life

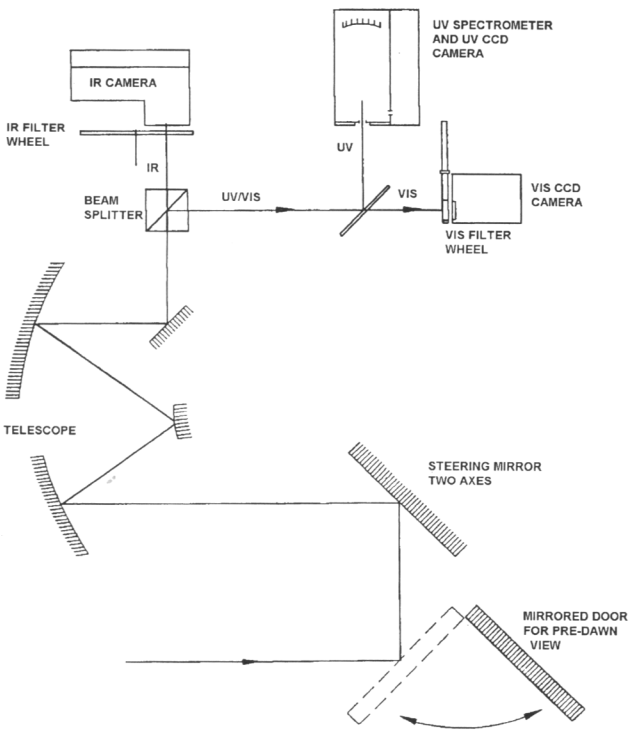

Figure 1. Sensor block diagram.

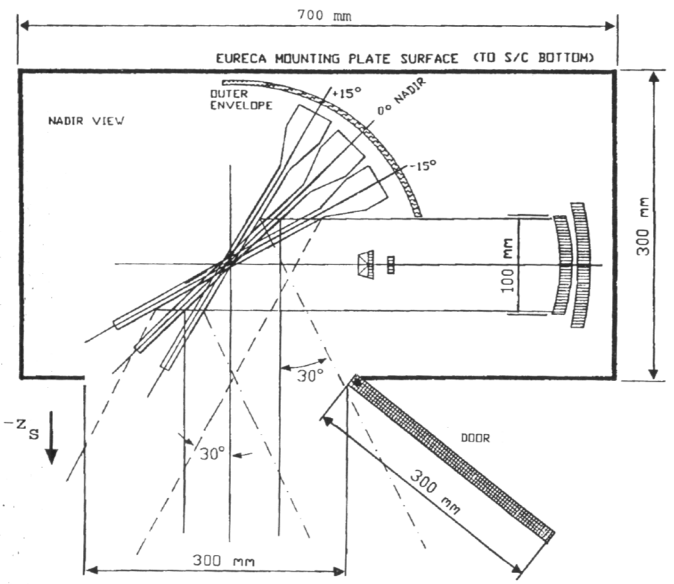

Figure 2. Nadir viewing operating mode. The mirrored door is held fully open and the steering mirror can be tilted within $[-15°, +15°]$ angle range.

sciences and radiobiology, as well as space science and technology research, and consequently, its orbit inclination and lifetime do not offer the appropriate coverage, the authors consider the EURECA mission an important opportunity to test the VEXUVIO sensor and a first step toward an operational free-flying mission.

EURECA has been designed to be launched and retrieved by the Space Shuttle. It will be deployed at the non-standard altitude of about 400 km and is scheduled for retrieval at an altitude of about 300 km. After deployment by the Orbiter, the EURECA on-board propulsion system will transfer the spacecraft to its nominal operational orbit of 515 km altitude, and 28·5° inclination. EURECA will perform flight missions of a typical duration from 6 to 9 months, during which it is always Sun-facing with a geometrically invariant attitude. After retrieval, the ESA satellite will return to its integration centre to be refurbished and re-equipped for another mission.

Since EURECA is Sun-pointing, VEXUVIO must be mounted on the satellite back-side, as shown in figure 4.

Taking into account the spacecraft orientation and VEXUVIO's pointing capability, the observational scenario is the following:

(*a*) During each orbit about $\frac{1}{4}$ of the equator is available for suitable viewing;
(*b*) For targets for which there is no viewing time restriction, the nadir near repeat cycle (NNRC) at about 515 km orbital altitude is 10 days. Because the orbital across-track separation is about 150 km, there is a three-day pre-nadir viewing period, one nadir day, and a three-day post-nadir viewing period. Thus, the NNRC cycle window of accessibility is 7 days viewing, 3 days off;
(*c*) For targets in the UV where the desired viewing window is $\pm 1{\cdot}5$ hours from local noon, the NNRC is 48 days. That is, 7 days of viewing followed by 41 days of inaccessibility;

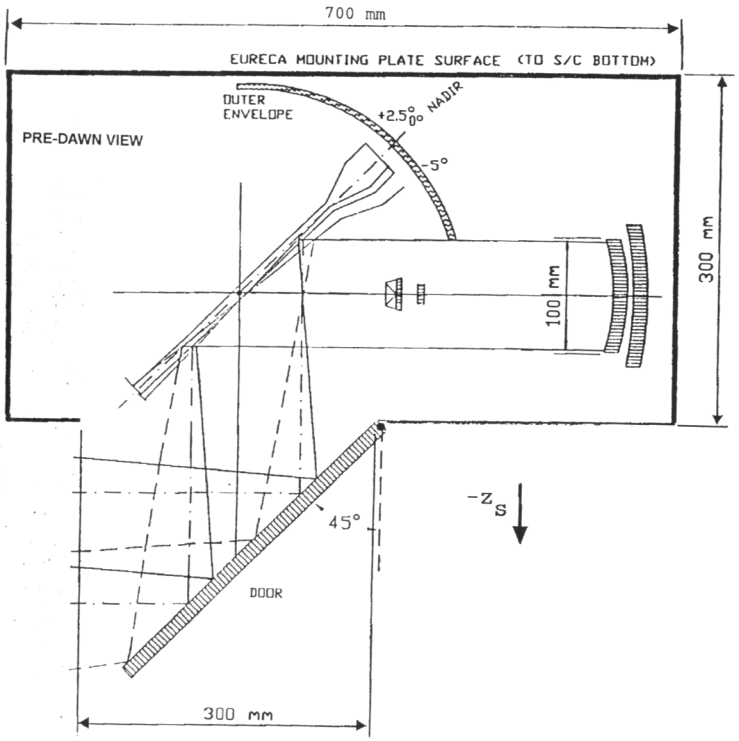

Figure 3. Pre-dawn operating mode. The mirrored door is held 45° tilted with respect to the $-z_s$ axis of EURECA and the steering mirror can be tilted with $[-5°, +2{\cdot}5°]$ angle range.

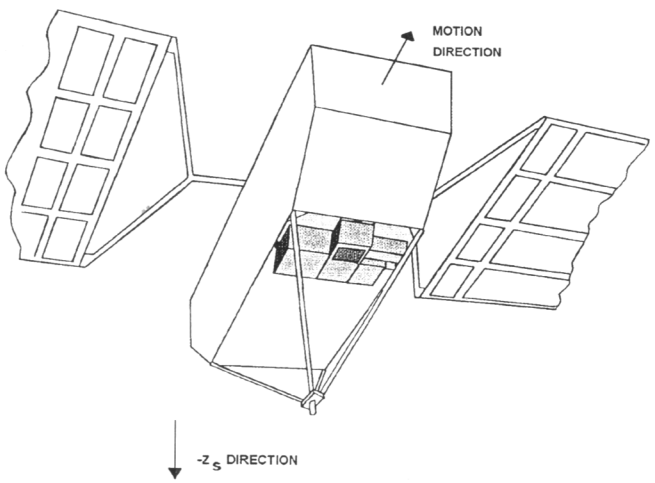

Figure 4. VEXUVIO possible accommodation on-board EURECA spacecraft.

(*d*) For targets where pre-dawn (up to −1 hour) observations are desired in near IR, the NNRC is much longer than 48 days, possibly a multiple of 2 or 3;
(*e*) 4050 stellar occultation opportunities (15 per day, 30 days per month, 6 to 9 months);
(*f*) In-flight calibration: stellar photometric calibrations.

The one day ground track of EURECA at 515 km orbital altitude and 0° first ascending node is shown in figure 5.

5. Simulation of VEXUVIO observation potential

In order to gain insight into the VEXUVIO observation potential, taking into account the mission scenario, a simulation program was developed to verify for how long and under what conditions volcanoes active during 1991 (table 1) are observable within the instrument pointing angle capability (range of tilt ±30°). Taking into account the operational limits of the satellite, the following simulation study is intended to verify the potentiality and the feasibility of EURECA/VEXUVIO mission.

5.1. *Analytical model*

The EURECA right-handed body fixed reference frame (x_s, y_s, z_s) is defined as follows: origin coincident with the spacecraft's centre of mass, z_s axis pointed

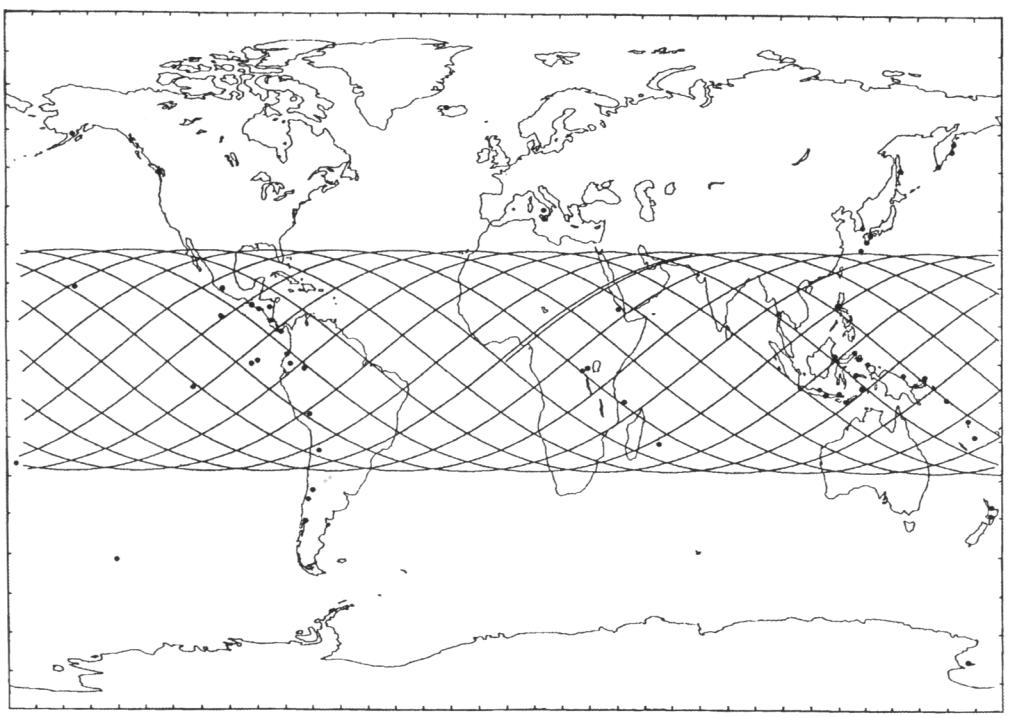

Figure 5. EURECA 1-day nadir track and geographic locations of the 59 volcanoes considered in our simulation programme and listed in table 1.

Table 1. List of the 59 volcanoes active during 1991.

Volcano	Latitude	Longitude	Volcano	Latitude	Longitude
Ambrym (Vanautu)	16·25° S	168·08° E	Marchena (Galapagos Is.)	0·33° S	90·46° W
Api Siau (Sangihe Is.)	2·78° N	125·48° E	Santa Maria (Guatemala)	14·76° N	91·55° W
Arenal (Costa Rica)	10·46° N	84·71° W	Monowai Seamount (Kermadec Is.)	25·89° S	177·19° W
Arjuno-Welirang (Java)	7·73° S	112·58° E	Nyamuragira (Zaire)	1·38° S	29·20° E
Aso (Kyushu)	32·88° N	131·10° E	Pacaya (Guatemala)	14·38° S	90·60° W
Avachincky (Kamchatka)	53·25° N	158·85° E	Pinatubo (Luzon)	15·14° N	120·35° E
Bagana (Boungainville)	6·14° S	155·19° E	Piton de la Fournaise (Reunion Is.)	21·23° S	55·71° E
Barren Island (Andaman Is.)	12·26° N	93·85° E	Planchon-Peteroa (Chile)	35·24° S	70·57° W
Cerro Hudson (Chile)	45·90° S	72·96° W	Poas (Costa Rica)	10·19° N	84·23° W
Colima (Mexico)	19·51° N	103·61° W	Raung (Java)	8·13° S	114·04° E
Ol Doinyo Lengai (Tanzania)	2·75° S	35·90° E	Redoubt (US-AK)	60·48° N	152·74° W
Dukono (Halmahera)	1·70° N	127·87° E	Ridge axis (East Pacific Rise)	9·80° N	104·29° W
Mt. Erebus (Antarctica)	77·53° S	167·16° E	Ricon de la Viejia (Costa Rica)	10·83° N	85·32° W
Erta Ale (Ethiopia)	13·60° N	40·67° E	Ruapehu (New Zealand)	39·28° S	175·57° E
Etna (Italy)	37·73° N	15·00° E	Ruiz (Colombia)	4·88° N	73·33° W
Fernandina (Galapagos Is.)	0·36° S	91·55° W	Sabancaya (Peru)	15·78° S	71·85° W
Galeras (Colombia)	1·21° N	77·36° W	Sakura-jima (Kyushu)	31·58° N	130·66° E
Gamalama (Ternate Is.)	0·80° N	127·33° E	Sangay (Ecuador)	2·03° S	78·33° W
Gunung Ranakah (Flores)	8·61° S	120·51° E	Semeru (Java)	8·11° S	112·92° W
Hekla (Iceland)	63·98° N	19·70° W	Shin-Iwo-jima (Volcano Is.)	24·28° N	141·52° E
Mt. St. Helens (US-WA)	46·20° N	122·18° W	Shiveluch (Kamchatka)	56·65° N	161·35° E
Iliboleng (Adonara)	8·34° S	123·26° E	Soputan (Sulawesi)	1·11° N	124·73° E
Karthala (Comoros Is.)	11·74° S	43·38° E	Stromboli (Italy)	38·79° N	15·21° E
Kavachi (Solomon Is.)	9·01° S	157·93° E	Suwanose-jima (Ryukyu)	29·53° N	129·72° E
Kilauea (US-HI)	19·43° N	155·29° W	Unnamed Seamount (S. Pacific)	53·90° S	140·30° W
Kliuchevskoi (Kamchatka)	56·06° N	160·64° E	Unzen (Kyushu)	32·75° N	130·30° E
Langila (New Britain)	5·53° S	148·41° E	Villarrica (Chile)	39·41° S	71·95° W
Lewotobi Lakilaki (Flores)	8·53° S	122·78° E	White Island (New Zealand)	37·52° S	177·18° E
Lokon-Empung (Sulawesi)	1·36° N	124·79° E	Yasur (Vanuatu)	19·51° S	169·43° E
Manam (Papua New Guinea)	4·10° S	145·06° E			

towards the Sun and y_s axis in the orbital plane. Because the instrument is designed to be mounted on the $-z_s$ axis of EURECA with its optical bench plane parallel to the (x_s, y_s) spacecraft plane and the axis perpendicular to the optical bench parallel to the spacecraft $-z_s$ axis, it is convenient to determine the pointing angles and all the quantities of interest with respect to the satellite body frame.

In the simulation model, we assume a keplerian circular orbit with parameters defined in a right-handed inertial reference frame (origin in the centre of the Earth, X-axis directed towards the first point of Aries and Z-axis towards North Pole, figure 6).

To calculate the transformation matrix, $\mathbf{M}$, from the inertial reference frame to the body reference frame, a right-handed orbiting reference frame is introduced, with origin in the spacecraft centre of mass, x-axis directed towards the position vector of the satellite and y-axis directed towards the satellite velocity vector. In this case, the transformation matrix $\mathbf{M}$ is then given by:

$$\mathbf{M} = \mathbf{M}_s \cdot \mathbf{M}_i \tag{1}$$

where $\mathbf{M}_s$ is the transformation matrix from the orbiting frame to the body frame and $\mathbf{M}_i$ is the transformation matrix from the inertial frame to the orbiting frame.

The transformation matrix $\mathbf{M}_i$ is computed by using Ω, the right ascension of the ascending node, ϕ, the geocentric angle between the ascending node and the position of the spacecraft, i.e., the anomaly with respect to the ascending node, and i, the satellite orbit inclination angle (Space Systems Division 1963):

$$\mathbf{M}_i = \begin{bmatrix} \cos\phi\cos\Omega - \sin\phi\sin\Omega\cos i & \cos\phi\sin\Omega + \sin\phi\cos\Omega\cos i & \sin\phi\sin i \\ -\sin\phi\cos\Omega - \cos\phi\sin\Omega\cos i & -\sin\phi\sin\Omega + \cos\phi\cos\Omega\cos i & \cos\phi\sin i \\ \sin\Omega\sin i & -\cos\Omega\sin i & \cos i \end{bmatrix} \tag{2}$$

For determining the matrix $\mathbf{M}_s$, it is necessary to know the components of the orbiting frame unit vectors in the body reference frame.

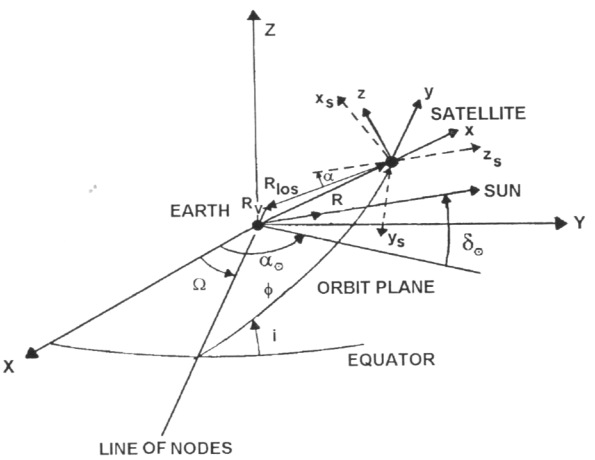

Figure 6. Geometry of the orbital mission.

The Sun unit vector $\mathbf{u}_\odot$ in an intertial reference frame is defined by its right ascension $\alpha_\odot$ and declination $\delta_\odot$ (H.M. Nautical Almanac Office 1961, Mugellesi and Van der Ha 1986):

$$\mathbf{u}_\odot = \cos\alpha_\odot \cos\delta_\odot \mathbf{I} + \sin\alpha_\odot \cos\delta_\odot \mathbf{J} + \sin\delta_\odot \mathbf{K} \tag{3}$$

where **I**, **J**, **K** are the unit vectors of the inertial frame axes.

Because of the Sun-pointing control and neglecting the Sun-pointing angle errors, the unit vector $\mathbf{u}_\odot$ is assumed to be coincident to the spacecraft z_s axis unit vector, $\mathbf{k}_s$. The unit vector $\mathbf{k}_s$ in the orbiting frame is given by (2).

$$\mathbf{k}_s = A\mathbf{i} + B\mathbf{j} + C\mathbf{k} \tag{4}$$

where **i**, **j** and **k** denote the unit vectors of the orbiting frame axes, and A, B, and C are:

$$\begin{cases} A = \cos\phi \cos\delta_\odot \cos\beta_\odot + \sin\phi \cos i \cos\delta_\odot \sin\beta_\odot + \sin\phi \sin i \sin\delta_\odot \\ B = -\sin\phi \cos\delta_\odot \cos\beta_\odot + \cos\phi \cos i \cos\delta_\odot \sin\beta_\odot + \cos\phi \sin i \sin\delta_\odot \\ C = -\sin i \cos\delta_\odot \sin\beta_\odot + \cos i \sin\delta_\odot \end{cases} \tag{5}$$

where $\beta_\odot = \alpha_\odot - \Omega$, i.e. it is the angle between the Sun and the spacecraft ascending node in the equatorial plane.

The body reference frame unit vector $\mathbf{j}_s$ is defined by the conditions to be perpendicular to the z_s axis and to lie in the orbital plane. It can be readily shown that $\mathbf{j}_s$ is given by:

$$\mathbf{j}_s = A'\mathbf{i} + B'\mathbf{j} + C'\mathbf{k} \tag{6}$$

where

$$\begin{cases} A' = \dfrac{B}{\sqrt{A^2 + B^2}} \\ B' = -\dfrac{A}{\sqrt{A^2 + B^2}} \\ C' = 0 \end{cases} \tag{7}$$

The components of the body reference frame unit vector $\boldsymbol{i}_s$ are computed considering the cross product and, then, the transformation matrix $\boldsymbol{M}_s$ becomes:

$$\mathbf{M}_s = \begin{bmatrix} -\dfrac{AC}{\sqrt{A^2 + B^2}} & -\dfrac{BC}{\sqrt{A^2 + B^2}} & \sqrt{A^2 + B^2} \\ \dfrac{B}{\sqrt{A^2 + B^2}} & -\dfrac{A}{\sqrt{A^2 + B^2}} & 0 \\ A & B & C \end{bmatrix} \tag{8}$$

After evaluating the matrix **M**, we are able to determine the sensor pointing angles with respect to the body reference frame.

If we know the geographical location of a volcano, and so its geodetic latitude (λ) and longitude (L), we can determine the components (X_v, Y_v, Z_v) of the volcano

Table 2. Orbital parameters used in the simulation programme are listed.

Semi-major axis:	6882·697 km	Ascending node local time:	21 June 1987 00:00:00
Orbit eccentricity:	0	Integration time:	1 sec
Orbit inclination:	28·5°	Number of orbits:	2900
Initial argument of perigee:	0°	Off-nadir pointing angle range:	±30°
Initial longitude of ascending node	0°		

position vector $\mathbf{R}_v$ in the inertial reference frame by using the following equations (Brooks 1977):

$$X_v = x_v \cos\alpha_g - y_v \sin\alpha_g$$
$$Y_v = x_v \sin\alpha_g + y_v \cos\alpha_g$$
$$Z_v = z_v$$

where α_g is the right ascension of Greenwich and x_v, y_v, z_v are given by:

$$x_v = \frac{a_\oplus}{\sqrt{1-e_\oplus^2 \sin\lambda \sin L}} \cos\lambda \cos L$$
$$y_v = \frac{a_\oplus}{\sqrt{1-e_\oplus^2 \sin\lambda \sin L}} \cos\lambda \sin L \qquad (10)$$
$$z_v = \frac{a_\oplus(1-e_\oplus^2)}{\sqrt{1-e_\oplus^2 \sin\lambda \sin L}} \sin\lambda$$

In these equations, $a_\oplus$ denotes the Earth major semi-axis and $e_\oplus$ denotes the Earth eccentricity computed considering the International Ellipsoid.

Hence, determining the satellite position vector components in the intertial reference frame by using the following equations:

$$X = p(\cos\phi \cos\Omega - \sin\phi \sin\Omega \cos i)$$
$$Y = p(\cos\phi \sin\Omega + \sin\phi \cos\Omega \cos i) \qquad (11)$$
$$Z = p(\sin\phi \sin i)$$

where p is the satellite orbit semi-latus rectum, we can evaluate the line of sight vector components in the intertial reference frame as follows (figure 6):

$$X_{los} = X_v - X$$
$$Y_{los} = Y_v - Y \qquad (12)$$
$$Z_{los} = Z_v - Z$$

and, therefore, the line of sight vector components in the body reference frame:

$$\begin{bmatrix} x_{s,los} \\ y_{s,los} \\ z_{s,los} \end{bmatrix} = \mathbf{M}_s \cdot \mathbf{M}_i \begin{bmatrix} X_{los} \\ Y_{los} \\ Z_{los} \end{bmatrix} \qquad (13)$$

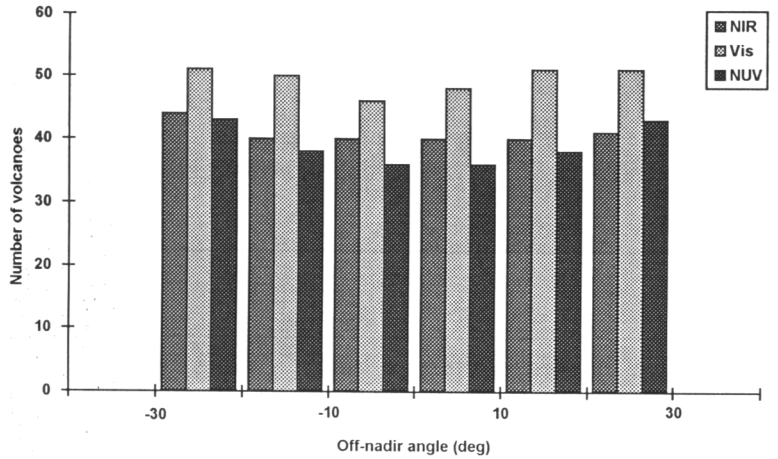
NIR
Vis
NUV
Number of volcanoes
60
50
40
30
20
10
0
-30
-10
10
30
Off-nadir angle (deg)

(*a*)

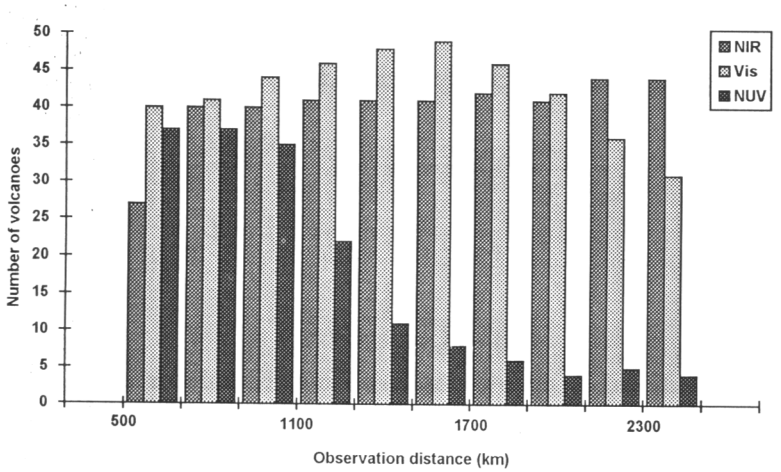
NIR
Vis
NUV
Number of volcanoes
50
45
40
35
30
25
20
15
10
5
0
500
1100
1700
2300
Observation distance (km)

(*b*)

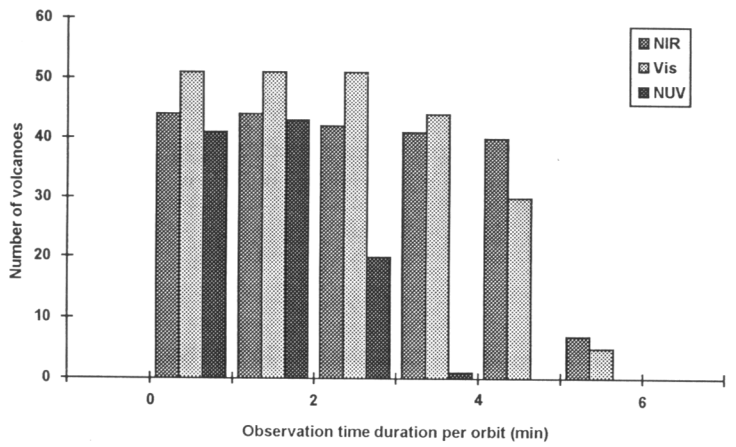
NIR
Vis
NUV
Number of volcanoes
60
50
40
30
20
10
0
0
2
4
6
Observation time duration per orbit (min)

(*c*)

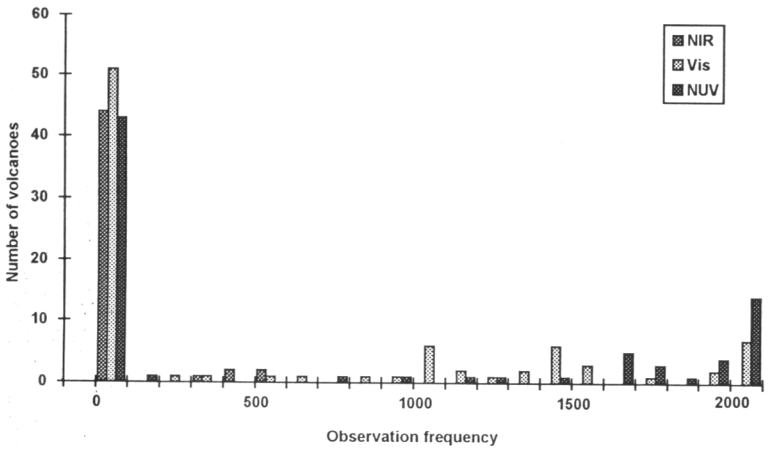

(*d*)

Figure 7 (*a*), (*b*), (*c*), (*d*). Numbers of volcanoes observed within contiguous intervals of: off-nadir pointing angle, observation distance, observation time duration per orbit, observation frequency, for each spectral band.

Finally, as shown in figure 6, we compute the off-nadir pointing angle with respect to the $-z_s$ axis:

$$\alpha = \cos^{-1}\left(\frac{z_{s,los}}{R_{los}}\right) \tag{14}$$

where $R_{los} = \sqrt{(x_{s,los})^2 + (y_{s,los})^2 + (z_{s,los})^2}$.

5.2. *Computer simulation results*

On the basis of the analytical model, the volcanoes listed in table 1 and the mission parameters listed in table 2, a computer simulation programme has been developed to analyse the observation potentiality of EURECA/VEXUVIO experiment.

Three observation time intervals have been chosen to increase the signal-to-noise ratio (S/N) for the different spectral ranges: $\pm 1{\cdot}5$ hours with respect to the local noon (NUV); 10 a.m. to 4 p.m. (Vis); 3 a.m. to 8 a.m. (NIR).

Taking into account the EURECA orbit inclination, only 50 volcanoes, among those considered in the simulation analysis (table 1) and located in the latitude range of $\pm 40^\circ$, were observable within the instrument pointing capabilities.

In order to get further insight into the potentiality of the system during the EURECA overall mission (2900 orbits, almost 6 months), the histograms of the following parameters have been plotted in figures 7 (*a*), 7 (*b*), 7 (*c*), and 7 (*d*) off-nadir pointing angle, observation distance (i.e., the distance between satellite and observed point), observation time duration per orbit and observation frequency (i.e., number of orbits between two successive observations). For the sake of clarity, these quantities have been quantized using an off-nadir angle of 10° as interval, 300 km as slant range interval, 1 minute as time interval, and 100 orbits as observation frequency interval. Consequently, figures 7 (*a*), 7 (*b*), 7 (*c*), and 7(*d*) are bar charts

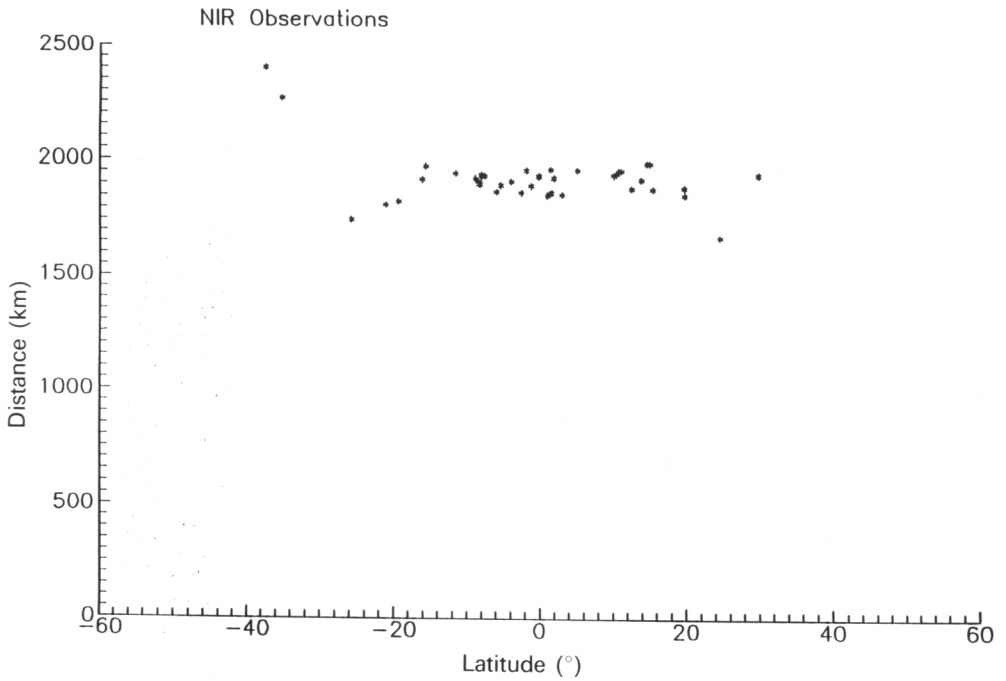
NIR Observations
2500
2000
1500
1000
500
0
Distance (km)
−60
−40
−20
0
20
40
60
Latitude (°)

(*a*)

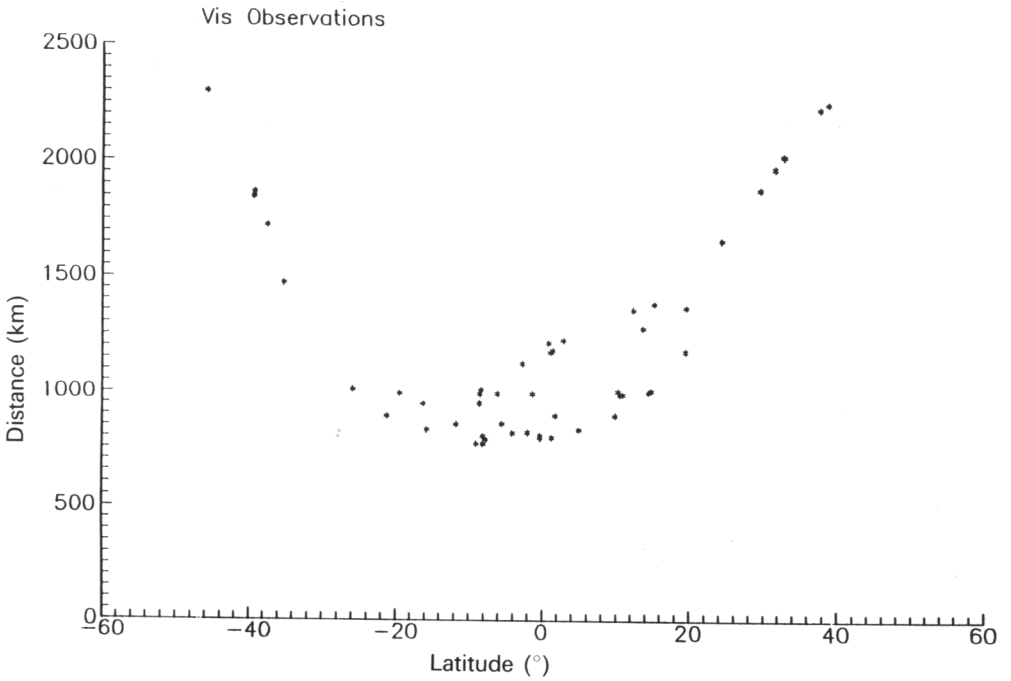
Vis Observations
2500
2000
1500
1000
500
0
Distance (km)
−60
−40
−20
0
20
40
60
Latitude (°)

(*b*)

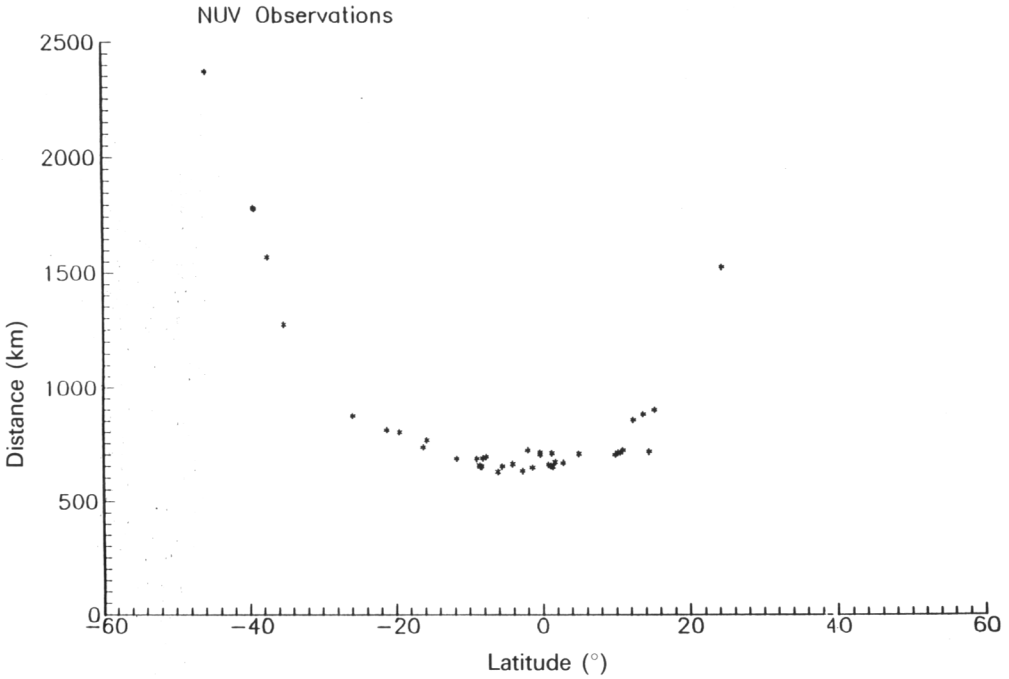

(*c*)

Figure 8 (*a*), (*b*), (*c*). Dependence of the mean observation distance on latitude for the three spectral bands (NIR, Vis, NUV).

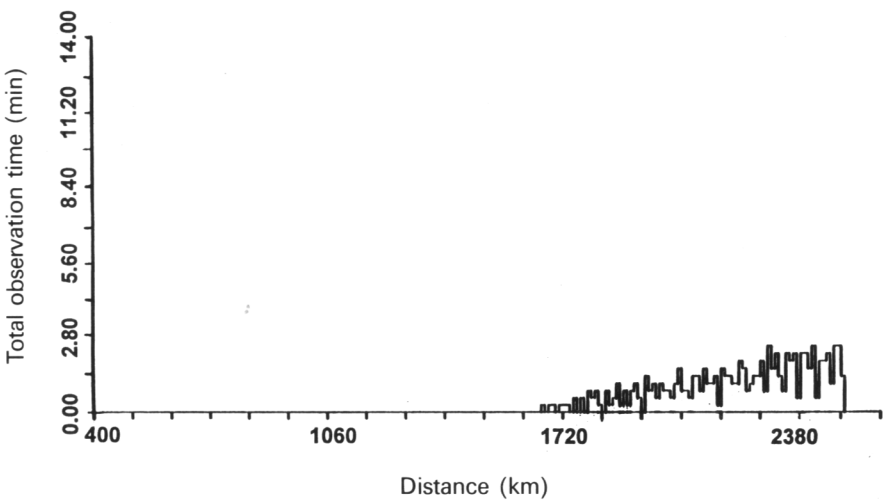

Figure 9. Total observation time duration at different distances in the case of Stromboli (Italy) volcano, Lat: 37·79° N Long: 15·21° E (Minimum Distance: 1664·50 km; Maximum Distance: 2496·73 km; Mean Distance: 2205·79 km; Standard Deviation: 206·45 km).

which show how many volcanoes are observed within these contiguous intervals for the three spectral bands (NIR, Vis, NUV). We selected these parameters to focus both technological and application oriented aspects of the proposed mission. In fact, the off-nadir pointing angle plot allows to evaluate the need and effectiveness of such capability, whereas the observation distance must be known for performing further studies connected to atmospheric absorption and scattering. Moreover, the observation time duration and the interval between two successive observations are connected to the potentiality of monitoring high and low frequency time-varying phenomena. Our results show that the pointing capability of the system is fully exploited (figure 7 (*a*)) and allows an observation time duration of several minutes per orbit (figure 7 (*c*)) with 4 days as maximum observation time interval between two successive observations in most cases (figure 7 (*d*)). The observation distance (figure 7 (*b*)) is mainly connected to the chosen observation time intervals for each spectral band. It is worth noting that the differences in the total number of volcanoes, among the three spectral bands within each parameter interval, are mainly due to the three different operational time intervals during each orbit: three, six, and five hours for NUV, Vis, and NIR, respectively.

The dependence of the mean observation distance as a function of the latitude is shown in figures 8 (*a*), (*b*), and (*c*) where each point represents one of the 50 accessible volcanoes. The volcanoes near the equator are observed at an average value of about 700 km in the NUV, which goes up to 1000 km in the Vis, and 1900 in the NIR, without considering any limitation given by cloud coverage and atmospheric transmittance. Since the *y*-axis scale has been chosen to put in evidence the potentiality of the system to observe the equatorial belt, which is the most favourite area because of the EURECA orbit inclination, some high-latitude volcanoes are outside the mean distance range.

As a worst case, the total observation time duration of the Stromboli volcano is plotted in figure 9. Since this volcano is located at 38·79° North latitude, it is the farthest North active volcano visible by EURECA/VEXUVIO. Figure 9 has been derived considering all the different slant ranges and spectral bands, during the whole mission. Although the minimum observation distance is quite high (1664 km), the total observation time still offers a good opportunity to acquire a time series of data of scientific interest with respect to the volcanic behaviour.

Actually, the number of observable targets and the mean observation distances can be reduced if problems related to cloud coverage and atmospheric transmittance are considered. With reference to the cloud cover profile reported by Peixoto and Oort (1991), the probability of penetrating through the atmosphere and of observing volcanic areas at low altitude can be roughly reduced of 50 per cent in near-IR and visible. Cloud coverage effects could be neglected in UV spectral band, since the low altitude observations are prevented by the ozone strong absorption and the high-power aerosols scattering. In fact, the UV measurements are referred to volcanic gases and aerosols ejected in stratosphere where cloudiness is very low.

6. Conclusion

In order to analyse the range of potential observations of the EURECA/VEXUVIO experiment, an analytical model has been developed. The simulation programme has shown that, in the case of 50 volcanoes which have been active during 1991, we get an observation frequency and time duration of scientific interest for studying the volcanic behaviour on a global scale. Although EURECA is not

primarily dedicated to Earth observations, the analysis conducted shows that the cost benefit of the proposed mission is satisfactory from the point of view of the expected scientific results.

Further activities, including deeper analysis on problems related to cloud coverage, atmosphere properties, and satellite coverage, will be concerned with the improvement of our computer program to simulate a dedicated volcanological mission of a free-flying mini-satellite to conduct an in-depth study of an Orbiting Volcano Observatory (OVO) (Penzo and Johnston 1992) that JPL has proposed within the NASA programme *Strategy for Earth Explorers in Global Earth Sciences* (National Research Council 1988).

Acknowledgments

This work was carried out in part at JPL under contract with the NASA Geology Program, and in part in Italy under Italian Space Agency contract.

References

ABBOTT, E. A., (editor), 1990, *Proceedings of the Second Thermal Infrared Multispectral Scanner (TIMS) Workshop 6 June 1990*, JPL Publication 90-55, NASA (Pasadena, California: Jet Propulsion Laboratory, California Institute of Technology).

ABRAMS, M. J., GLAZE, L. S., and SHERIDAN, J., 1991, Monitoring Colima Volcano, Mexico, using satellite data. *Bulletin of Volcanology*, **59,** 571-574.

BIANCHI, R., CASACCHIA, R., CORADINI, A., DUNCAN, A. M., GUEST, J. E., KAHLE, A., LANCIANO, P., PIERI, D. C., and POSCOLIERI, M., 1990, Remote Sensing of Italian volcanos. *EOS Transactions*, **71,** 1789-1791.

BROOKS, D. R., 1977, An introduction to orbit dynamics and its application to satellite-based Earth monitoring missions, NASA Reference Publication 1009 (Hampton, Virginia: Langley Research Center).

CASADEVALL, T. J., JOHNSTON, D. A., HARRIS, D. M., ROSE, W. I., MALINCONICO, L. L., STOIBER, R. E., BORNHORST, T. J., WILLIAMS, S. N., WOODRUFF, L., and THOMPSON, J. M., 1990, SO_2 emission rates at Mount St. Helens from March 29 through December, 1990. *U.S. Geological Survey Professional Paper 1250*, pp. 193-200.

FARRAND, W. H., and SINGER, R. B., 1991, Analysis of altered volcanic pyroclasts using AVIRIS data, *Proceedings of the Third Airborne Visible/Infrared Imaging Spectrometer (AVIRIS) Workshop, 20 and 21 May 1991*, JPL Publication 91-28, NASA, pp. 248-255.

HAULET, R., ZETTWOOG, P., and SABROUX, J. C., 1977, Sulphur dioxide discharge from Mount Etna. *Nature*, **268,** 715-717.

H.M. NAUTICAL ALMANAC OFFICE, 1961, *Explanatory Supplement to the Astronomical Ephemeris and the American Ephemeris and Nautical Almanac, prepared jointly by the Nautical Almanac Offices of the United Kingdom and the United States of America* (London: Her Majesty's Stationery Office).

KRUEGER, A. J., 1983, Sighting of El Chichon sulphur dioxide clouds with the Nimbus-7 Total Ozone Mapping Spectrometer. *Science*, **220,** 1377-1379.

MALINCONICO, L. L. JR, 1979, Fluctuations in SO_2 emission during recent eruptions of Etna. *Nature*, **278,** 43-45.

MOUGINIS-MARK, P. J., PIERI, D. C., FRANCIS, P. W., WILSON, L., SELF, S., ROSE, W. I., and WOOD, C. A., 1989, Remote Sensing of volcanoes and Volcanic terrains. *EOS Transactions*, **70,** 1570-1572.

MOUGINIS-MARK, P. J., ROWLAND, S., FRANCIS, P., FRIEDMAN, T., GARBEIL, H., GRADIE, J., SELF, S., WILSON, L., CRISP, J., GLAZE, L., JONES, K., KAHLE, A., PIERI, D., ZEBKER, H., KREUGER, A., WALTER, L., WOOD, C., ROSE, W., ADAMS, J. and WOLF, R., 1991, Analysis of active volcanoes from the Earth Observing System. *Remote Sensing of Environment*, **36,** 1-12.

MUGELLESI, R., and VAN DER HA, J. C., 1986, RIT-10 Low-Thrust Control of EURECA's Orbital Decay. *ESA Journal*, **10,** 59-70.

NATIONAL RESEARCH COUNCIL, 1988, Strategy for Earth Explorers in Global Earth Sciences, Space Science Board (CES) Report (Washington DC: National Academy Press).

NELLESSEN, W., 1991, EURECA System Overview, ESA Estec, Doc No. ERC-PL-111-0, Issue 2.0, January 1991.

NELLESEN, W., 1986, The EURECA Design Concept. *ESA Bulletin*, **47,** 7–14.

OPPENHEIMER, C., 1991, Lava flow cooling estimated from Landsat Thematic Mapper infrared data: the Lonquimay eruption, Chile, 1989. *Journal of Geophysical Research*, **96,** 21856–21878.

OPPENHEIMER, C., and ROTHERY, D. A., 1991, Infrared monitoring of volcanoes by satellite, *Journal of the Geological Society London*, **148,** 563–569.

OPPENHEIMER, C., FRANCIS, P. W., ROTHERY, D. A., CARLTON, R. W., and GLAZE, L. S., 1993, Interpretation and comparison of volcanic thermal anomalies in Landsat Thematic Mapper infrared data: Volcan Lascar, Chile, 1984–1991. *Journal of Geophysical Research* (in press).

PEIXOTO, J. P., and OORT, H. A., 1991, *Physics of Climate* (New York: American Institute of Physics).

PENZO, P. A., and JOHNSTON, M. D., 1992, Mission Design for an Orbiting Volcano Observatory. *Journal of Spacecraft and Rockets*, **29,** 502–507.

PIERI, D. C., GLAZE, L. S., and ABRAMS, M. J., 1990, Thermal radiance observations of active lava flow during the June 1984 eruption of Mount Etna. *Geology*, **18,** 1018–1022.

ROTHERY, D. A., FRANCIS, P. W., and WOOD, C. A., 1988, Volcano monitoring using short wavelength infrared data from satellite. *Journal of Geophysical Research*, **93,** 7993–8008.

ROTHERY, D. A., and OPPENHEIMER, C. M. M., 1991, Monitoring volcanoes using short wavelength infrared images. *Proceedings 5th International Colloquium on Spectral Signatures of Objects in Remote Sensing, Courchevel, France 14–18 January 1991*, ESA SP-319 (Noordwijk, The Netherlands: ESA Publications Division, European Space Research and Technology Centre), pp. 513–516.

ROTHERY, D. A., and PIERI, D. C., 1993, Remote sensing of active lava, Monitoring Active Lavas edited by C. J. Kilburn (London: UCL Press) (to be published).

SPACE SYSTEMS DIVISION OF THE MARTIN COMPANY, 1963, Orbital Flight Handbook, NASA SP 33 Part 1, prepared for the G. C. Marshall Space Flight Center, Huntsville, Alabama, U.S.A.